Design and Implementation of Early Warning Monitoring System for Cross-border Mining in Open-pit Mines

Li Ke[1], Byung-Won Min[2*]
[1]Ph.D. Student, Division of Information and Communication Convergence Engineering, Mokwon University
[2]Professor, Division of Information and Communication Convergence Engineering, Mokwon University

노천광산의 월경 채굴 조기경보 모니터링시스템의 설계 및 구현

이크[1], 민병원[2*]
[1]목원대학교 정보통신융합공학부 박사과정, [2]목원대학교 정보통신융합공학부 교수

Abstract For the scenario of open pit mining, at present, manual periodic verification is mainly carried out in China with the help of video surveillance, which requires continuous investment in labor cost and has poor timeliness. In order to solve this difficult problem of early warning and monitoring, this paper researches a spatialized algorithmic model and designs an early warning system for open-pit mine transboundary mining, which is realized by calculating the coordinate information of the mining and extracting equipments and comparing it with the layer coordinates of the approval range of the mines in real time, so as to realize the determination of the transboundary mining behavior of the mines. By taking the Pingxiang area of Jiangxi Province as the research object, after the field experiment, it shows that the system runs stably and reliably, and verifies that the target tracking accuracy of the system is high, which can effectively improve the early warning capability of the open-pit mines' overstepping the boundary, improve the timeliness and accuracy of mine supervision, and reduce the supervision cost.

Key Words : Open-pit mine; Cross-border mining; Image processing; Spatial coordinates; Early warning monitoring.

요 약 노천 광산 채굴 시나리오와 관련하여 현재 중국에서는 주요 수동 및 정기 검사를 위한 비디오 모니터링을 사용하는 것으로 인건비를 지속적으로 투자해야 하며 적시성이 낮다. 이 조기경보 모니터링의 문제를 해결하기 위해 이 글에서는 공간화 알고리즘 모델을 개발하여 노천광산의 월경채굴 조기경보시스템을 설계하고 광산채굴장비의 지리적 정보를 산출하고 실시간으로 광산 승인 범위의 레이어 좌표와 비교하고, 자동으로 광산의 월경 채굴 행동을 예측한다. 장시 핑샹 지역을 연구 대상으로 하여 노천 광산 채굴 엔지니어링 기계 장비를 식별 및 추적 대상으로 선정하였으며, 현장 실험을 통해 시스템이 안정적이고 신뢰할 수 있으며 검증 시스템의 목표 추적 정확도가 높은 것으로 나타났으며, 광산 채굴 감독의 적시성과 정확성을 향상시킬 수 있고 감독의 인건비를 크게 절감할 수 있다.

주제어 : 노천 광산, 월경 채굴, 이미지 처리, 공간 좌표, 조기 경보 및 모니터링

*교신저자 : 민병원(minfam@mokwon.ac.kr)
접수일 2024년 02월 28일 수정일 2024년 03월 07일 심사완료일 2024년 03월 21일

1. Introduction

China's mineral resources are owned by the state. According to the needs of strategic development, the state issues mineral resources mining licenses to relevant units or individuals to better serve the country's economic development through reasonable and orderly mining. However, in recent years, driven by economic interests, some illegal mining elements have wantonly carried out cross-border mining and illegal mining without obtaining a mineral resources exploitation license or on the basis of obtaining a mineral resources exploitation license, secretly exploiting the country's mineral resources, resulting in serious losses of the country's mineral resources [1].

At present, illegal mining supervision mostly adopts the method of "step-by-step statistical reporting, mass reporting, on-site inspection", which to some extent leads to long cycle, poor timeliness, great influence of human factors, low accuracy. as a result, it is difficult to supervise some illegal mining, affect the normal mining order of mines, form hidden dangers of safety accidents and seriously damage the environment [2]. Therefore, the effective supervision of mines is the primary condition to ensure the orderly exploitation of mineral resources, in which the main objects of open-pit mining supervision are cross-border mining and illegal mining.

Pingxiang City is rich in mineral resources, which is famous for its rich mineral resources in history. The proved mineral deposits are rich in coal, iron, manganese, copper, limestone, kaolin, silty quartz, porcelain clay and other mineral resources. 285 mineral areas have been found and 87 industrial deposits have been discovered. According to the reserves of retained resources, there are 6 medium-sized, 81 small-sized, 162 ore spots and 36 mineralization points [3]. Pingxiang is a city based on coal, Pingxiang Coal Mine is the first coal mine in the south of the Yangtze River to use Western machinery to produce, transport, wash coal and make coking. However, Pingxiang is mostly mountainous and hilly, the mining area is mainly distributed in the more remote mountain areas, the distribution is more scattered, illegal mining often occurs. These factors not only greatly increase the difficulty of supervision of mining areas, but also require higher monitoring costs, and lead to serious ecological vulnerability problems.

Taking Pingxiang area of Jiangxi Province as the research object, this paper selects the engineering machinery equipment of open-pit mining as the identification and tracking object, mainly trucks, excavators, bulldozers, road rollers and so on [4]. Based on photogrammetry technology and Zhang Zhengyou calibration method [5], the aerial view coordinate transformation of video angle is creatively deduced, and a video spatialization algorithm is constructed on the basis of verifying camera calibration experiment. An intelligent early warning system for cross-border mining in open-pit mines is studied and designed. Combined with the actual case of field application, the coordinates of mining equipment are located and tracked by video image, and compared with the layer coordinates of mine examination and approval scope in real time, so as to realize the prediction and alarm of cross-boundary mining in open-pit mine [6]. It is of great significance to standardize open-pit mining by providing convenience and support for regulatory departments.

2. Related technologies

2.1 Photogrammetric technology

Photogrammetry is a branch of surveying and mapping, which measures the position coordinates and motion patterns of objects in three- dimensional space through two-dimensional images taken by cameras. It mainly studies the use of cameras and computers to identify, track, measure targets

and other related functions. Photogrammetry not only includes image processing, target reconstruction, recognition and analysis, but also can obtain three-dimensional information of the research scene according to the processed video images. This function is called 3D reconstruction [7].

Choy et al. (2016) designed a three-dimensional (3-dimen-sional, 3D) long short term memory (LSTM) network based on LSTM to process the coded information of a single image, and realized end-to-end reconstruction of a 3D model from a single image [8]. Yang et al. (2019) utilized generative adversarial network (GAN) to improve the voxel model reconstruction network, but it requires simultaneous input of depth maps, which increases the difficulty of obtaining the input information [9]. Liu et al. (2018) used a 3D convolutional neural network for encoding, which replaces the 2D convolution in the decoder with a 3D convolution, which can be adapted to the 3D model, and the learned potential features decoded as 3D occupancy probabilities thus reconstructing the voxel model [10]. Tulsiani et al. (2017, 2018) used multi-view 2D images and corresponding mask images as a baseline, trained the network using view consistency loss to reduce the difficulty of data acquisition, and utilized a single image to predict voxel occupancy probabilities and reconstruct the voxel model of an object [11]. Yu and Oh (2022) trained a variational self-encoder using category-specific multimodal prior distributions in the latent space, and using a subset of the latent space it is possible to find the target modality of the prior distribution and obtain prior information about the category [12]. By using the voxel model, the 2D convolution used in image analysis can be easily extended to 3D.

The image information collected by existing means is always expressed by two-dimensional digital matrix, but the real geographical space contains three-dimensional scale. Therefore, we need to reasonably extract the relevant information from the two-dimensional image and express the three-dimensional information of the model, and the main method to realize this technology is three-dimensional reconstruction technology. Before the target reconstruction, the first thing that needs to be carried out is to calibrate the camera used to collect the image, which is also called camera calibration. Calibration is mainly carried out by the following three methods: traditional camera calibration methods (such as direct linear transformation DLT), self-calibration methods, and camera calibration methods based on active vision [13].

The calibration technology has been constantly updated for many years, and a large number of advanced, effective and applicable calibration methods have been put forward. Zhang Zhengyou calibration method is one of the classic methods. A complete photogrammetry system usually consists of three parts, namely, digital image acquisition, camera calibration and image processing. This method combines the traditional method and the self-calibration method, and uses the single-plane checkerboard method for camera calibration [14]. Compared with the traditional method, it does not need a high-precision calibration object, but only through a printed checkerboard. At the same time, compared with self-calibration, it improves the accuracy and is easy to operate, so it is widely used in the field of photogrammetry.

2.2 Keyhole imaging principle

In the late Spring and Autumn period and early warring States period in China, Mo Zhai, a scholar of the Song Dynasty and his students, recorded in the Mojing that after the sun shines on the human body, the light at the boundary of the body shoots forward like an arrow, and the light from the lower part of the body hits the upper part of the screen. the light from the upper part of the body hits the lower part of the screen. The reason for this phenomenon is that there is a small hole in the path of light

propagation, the light from the foot is blocked by the lower part of the body, the light from the head is blocked by the upper part of the body, and a bright inverted image appears in the dark box after passing through the hole. The experimental method also proves the property of light propagating along a straight line. As shown in figure 1, this is the keyhole imaging schematic [15].

Modern digital cameras make use of the principle of keyhole imaging. The zoom lens is the keyhole O, the object being measured hits the imaging plane through the keyhole as the camera image plane, and the distance from the keyhole to the camera image plane is the focal length f.

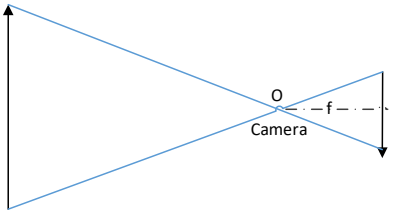

[Fig. 1] Keyhole imaging schematic diagram

2.3 PNPoly arithmetic

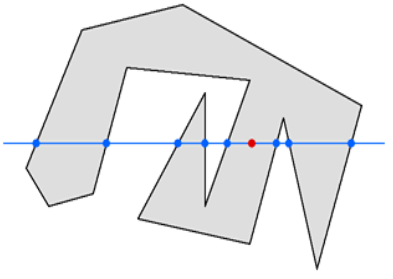

[Fig. 2] Schematic diagram of intersection of points in PNPoly algorithm

According to W. Randolph Franklin, In the proposed PNPoly algorithm, the polygon divides the plane into inner and outer regions. Assuming that the test point is inside the polygon, a ray drawn from the test point must have at least one intersection with the polygon [16]. The ray will "rush out" the polygon the first time it intersects with the polygon, and "enter" the polygon the second time, and so on. If the ray has an odd number of intersecting points with the polygon, the point is inside the polygon and vice versa, as shown in figure 2.

3. Research on the conversion algorithm of each coordinate system

In the camera model of computer vision, each camera involves four coordinates, namely, the world coordinates, the camera coordinates, the image coordinates and the pixel coordinates [17]. The imaging process is shown in figure 3.

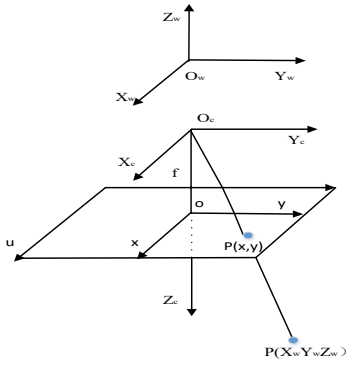

[Fig. 3] Spatial coordinate correspondence diagram of camera model

(1) World coordinates: $O_w - X_w W_w Z_w$, P point is a point in the world coordinates, that is $P(X_w Y_w Z_w)$, a real point in life ;

(2) Camera coordinates : $O_c - X_c W_c Z_c$, Where O_c is the focus of the image plane, and the X_c and Y_c axes are parallel to the long and short axes of the image, respectively, and are the coordinates of point $P(X_c Y_c Z_c)$ in the direction of the camera space coordinates ;

(3) Image coordinates : o-xy , Where o is the vertex on the upper left of the image, the x axis is parallel to the long axis of the image, the y axis is parallel to the short axis of the image,

and p (x, y) is the imaging point of point P in the image ;

(4) Pixel coordinates : o-uv, The u axis is parallel to the image's long axis, and the v axis is parallel to the short axis.

When converting a three-dimensional point in the world coordinates to a two-dimensional image in pixels, the usual forward projection process is to first convert the point in the world coordinates to the camera coordinates according to the external parameter matrix, and then through the camera internal parameter (camera focal length) parameter, that is, the length of the origin O_c-o of the two coordinates is the focal length (let the lower focal length be f and the magnification is z, The focal length is = zf), which converts the points in the camera coordinates to the image coordinates;Then the center point of the imaging coordinates is translated to the center point of the pixel coordinates through the camera internal reference O_x, O_y,. Finally, according to S_x, S_y(image sampling rate in the x-axis and y-axis direction), the imaging coordinates is converted to the image coordinates.

3.1 Conversion between world coordinates and camera coordinates

The transformation of these two coordinates belongs to rigid-body transform, which only needs rotation and translation $(R,\vec{t})$, and the transformation relationship is shown in figure 4.

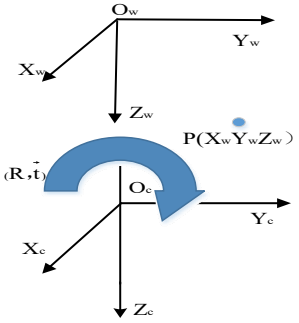

[Fig. 4] Conversion diagram between world coordinates and camera coordinates

The conversion parameters are represented by the rotation matrix R and the translation matrix $\vec{t}$, so the coordinates of point P in the camera coordinates are shown in formula (1.1).

$$\begin{bmatrix} X_c \\ Y_c \\ Z_c \\ 1 \end{bmatrix} = \begin{bmatrix} R\ t \\ \vec{0}\ 1 \end{bmatrix} \begin{bmatrix} X_W \\ Y_w \\ Z_W \\ 1 \end{bmatrix} \quad (1.1)$$

Where R is 3 × 3 matrix and t is 3 × 1 matrix , $\vec{0}\ [0,0,0]$.

3.2 Conversion between camera coordinates and Image coordinates

The imaging relationship from the camera coordinates to the image coordinates is perspective projection, and the three-dimensional information points are projected onto the two-dimensional image coordinates. According to the linear camera model based on pinhole model, the coordinates can be obtained as shown in figure 5, and the transformation formula is represented by equation (1.2).

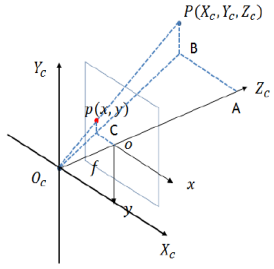

[Fig. 5] Conversion diagram between camera coordinates and image coordinates

$$x = f\frac{X_c}{Z_c} \qquad y = f\frac{Y_c}{Z_c} \quad (1.2)$$

Convert to matrix form such as formula (1.3) :

$$Z_c\begin{bmatrix} x \\ y \\ 1 \end{bmatrix} = \begin{bmatrix} f\ 0\ 0\ 0 \\ 0\ f\ 0\ 0 \\ 0\ 0\ 1\ 0 \end{bmatrix} \begin{bmatrix} Xc \\ Yc \\ Zc \\ 1 \end{bmatrix} \quad (1.3)$$

3.3 Conversion between Image coordinates and pixel coordinates

Both the image coordinates and the pixel coordinates are on the imaging plane, but their origin and unit of measurement are different. The origin of the image coordinates is the intersection of the camera optical axis and the imaging plane, and generally the midpoint of the imaging plane. The relationship between the two coordinates is shown in figure 6.

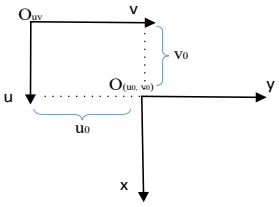

[Fig. 6] Conversion diagram between image coordinates and pixel coordinates

The unit of the image coordinates is mm, which belongs to the physical unit, and the unit of the pixel coordinates is pixel, which is what we usually call pixels. Assuming that the physical dimensions of each pixel in the u-axis and v-axis directions are d_x and d_y, respectively, their dimensions are converted as shown in the formula (1.4).

$$u = \frac{x}{dx} + u0 \qquad v = \frac{y}{d_y} + v_0 \tag{1.4}$$

d_x and d_y are the actual dimensions of each pixel on the chip. According to this relationship, the relationship between the pixel coordinates and the real coordinate is established. u_0 and v_0 represent the center of the pixel plane. The matrix representation of the above formula is shown in the formula (1.5).

$$\begin{bmatrix} u \\ v \\ 1 \end{bmatrix} = \begin{bmatrix} \frac{1}{dx} & 0 & u_0 \\ 0 & \frac{1}{dy} & v_0 \\ 0 & 0 & 1 \end{bmatrix} \begin{bmatrix} x \\ y \\ 1 \end{bmatrix} \tag{1.5}$$

In summary, the transformation from the world coordinates $P(X_w, Y_w, Z_m, 1)^T$ of the spatial 3D point P to the pixel coordinate $p(u, v, 1)^T$ of its corresponding projection point p in the image plane can be divided into three transformations, as shown in figure 7.

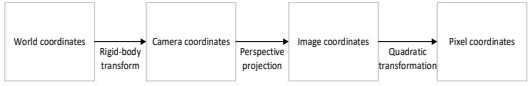

[Fig. 7] The conversion relationship between coordinates

That is, the world coordinates can be transformed into camera coordinates by rigid-body transformation, the camera coordinates can be transformed into image coordinates by perspective projection, and the image coordinates can be transformed into pixel coordinates by secondary transformation, so as to complete the conversion calculation of each coordinate.

3.4 Conversion between pixel coordinates and world coordinates

Through the transformation of the above four coordinate systems, the transformation relationship of a point from the world coordinates to the pixel coordinates can be deduced, as shown in the formula (1.6).

$$Z_c \begin{bmatrix} u \\ v \\ 1 \end{bmatrix} = \begin{bmatrix} \frac{1}{d_x} & 0 & u_0 \\ 0 & \frac{1}{d_y} & v_0 \\ 0 & 0 & 1 \end{bmatrix} \begin{bmatrix} f & 0 & 0 & 0 \\ 0 & f & 0 & 0 \\ 0 & 0 & 1 & 0 \end{bmatrix} \begin{bmatrix} R & t \\ \rightarrow & \\ 0 & 1 \end{bmatrix} \begin{bmatrix} X_w \\ Y_w \\ Z_w \\ 1 \end{bmatrix}$$

$$= \begin{bmatrix} f_x & 0 & u_0 & 0 \\ 0 & f_y & v_0 & 0 \\ 0 & 0 & 1 & 0 \end{bmatrix} \begin{bmatrix} R & t \\ \vec{0} & 1 \end{bmatrix} \begin{bmatrix} X_w \\ Y_w \\ Z_w \\ 1 \end{bmatrix} = M_1 M_2 X_w = M X_w \tag{1.6}$$

Among them, M_1 is the internal number of the camera, which is only related to the structure of the camera; M_2 (that is, R and $\vec{t}$) is the external parameters of the camera, and the external parameters of the camera are determined by the azimuth relationship between the camera itself and the world coordinates. These parameters need to be obtained by camera calibrations.

It can be seen from equation 1.6 that a three-dimensional coordinate point under real-world coordinates can be converted to its corresponding pixel in the image, and at the same time, without considering the elevation of the coordinate point, through a point in the image, the two-dimensional geographical coordinates of the corresponding point in the real space can also be found.

3.5 Coordinate algorithm of actual measuring area and video viewing angle

In addition to paying attention to the conversion relationship between the world coordinates, camera coordinates, image coordinates and pixel coordinates, we also need to pay attention to the coordinate transformation relationship between the actual measurement area and the video viewing angle. Combined with Zhang Zhengyou's calibration method, we creatively derive the aerial view coordinate transformation of the video perspective.

The world coordinates of the four vertices reconstructed from the aerial view of the video can approximately form the measured rectangular area, that is, the actual measured area corresponds to the four vertex coordinates of the aerial view [18], as shown in figure 8 :

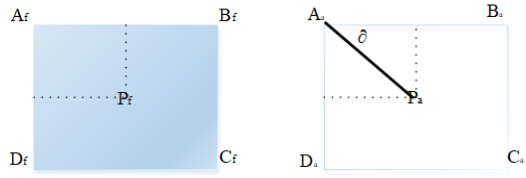

[Fig. 8] Coordinate conversion between actual measuring area and aerial View

The coordinates of the four vertices of the known actual measurement area are respectively $A(A_{fx},A_{fy})$, $B(B_{fx},B_{fy})$, $C(C_{fx},C_{fy})$, $D(D_{fx},D_{fy})$, and the coordinates of the four vertices in the aerial view are $A(A_{ax},A_{ay})$, $B(B_{ay},B_{ay})$, $C(C_{ax},C_{ay})$, $D(D_{ax},D_{xy})$. Then the conversion relationship between point $P_a(P_{ax},P_{ay})$ on the aerial view and its corresponding point $P_f(P_{fx},P_{fy})$ in the actual measurement area satisfies the following formula (1.7) :

$$\begin{aligned} P_{fx} &= A_{fx} + S\left(P_{ax}^2 + P_{ay}^2\right)^{1/2}\cos\partial \\ P_{fy} &= A_{fy} + S\left(P_{ax}^2 + P_{ay}^2\right)^{1/2}\sin\partial \end{aligned} \tag{1.7}$$

Among them, the scale coefficient S of the actual measurement area and aerial view can be solved by the following formula (1.8) :

$$S = \frac{\sqrt{(A_{fx}-B_{fx})^2 + (A_{fy}-B_{fy})^2}}{B_{ax}} \tag{1.8}$$

3.6 PNPoly algorithm design

The PNPoly algorithm draws a horizontal ray to the right from the monitoring point, and calculates the number of intersecting points with the polygon, such as formula (1.9). In the formula (1.9), xpene y is the coordinates of polygon vertices, x' and y' are the arrays of horizontal and vertical coordinates of polygon vertices respectively, and x'' and y'' are the coordinates of the monitored points.

$$y-y'=\frac{y'[j]-y'[i]}{x'[j]-x'[i]}(x-x'[i]) \qquad (1.9)$$

The formula under change (2.0) :

$$x=\frac{(x'[j]-x'[i])(y-y'[i])}{y'[j]-y'[i]}+x'[i] \quad (2.0)$$

Substitute the coordinates of the points to be monitored, and get this inequality (2.1) according to the graphical relationship :

$$x''<\frac{(x'[j]-x'[i])(y-y'[i])}{y'[j]-y'[i]}+x'[i] \quad (2.1)$$

According to the formula, the core code designed is shown in Table 1 :

〈Table 1〉 Core code implementation of PNPoly algorithm design

```
private static int n = 0; // Number of polygonal vertices
private static int[] x = new int[20]; // Polygonal vertex coordinates
private static int[] y = new int[20];
private static int x'' = -1, y'' = -1; // Test point coordinates
public static boolean pnploy(int x'', int y'') { // The PNplot algorithm is
used to determine whether the point is in the polygon.
        boolean result = false;
        for (int i = 1, j = n; i <= n; j = i++) {
            if (((y[i] > y'') != (y[j] > y'')) && (x'' < (x[j] - x[i]) * (y'' - y[i])
* 1.0 / (y[j] - y[i]) + x[i])) {
                result = !result;
            }
        }
        return result;
    }
```

Explain this code:for (i = 1, j = n; i <=n; j = i++)The meaning of a loop is to always let j = i-1 , If I = 0 then j = n-1, then check each edge of the polygon in turn.

The next key point is the conditional statement, (y[i]>y'') != (int[j]>y''). It is easy to understand that the two vertices of an edge are above and below the monitored point, respectively. Through this statement, we can know that the ray to the right from the monitored point may intersect the edge (as long as the monitored point is on the left side of the edge).

That is, x'' < (x[j] - x[i]) * (y'' - y[i]) * 1.0 / (y[j] - y[i]) + x[i]) to realize the graph relation inequality of PNPoly algorithm.

4. Camera calibration experiment

In the process of digital photogrammetry, in order to determine the relationship between the three-dimensional geometric position of a point on the surface of a space object and its corresponding point in the image, the geometric model of camera imaging must be established. These geometric model parameters are camera parameters, including camera internal and external parameters [19].

The internal geometric structure and light characteristics of the camera are the internal parameters of the camera, and the geometric transformation relationship between the camera coordinates and the world coordinates is the external parameters of the camera. In general, these parameters have to be obtained according to experiments and calculations, and the process of solving the parameters is called camera calibration. The algorithm steps for verification are as follows:

1.Collect image data: first you need to use the camera to obtain multiple pictures containing known objects or specific patterns.

2.Extract corners: extract corners from each picture (the grid of calibration paper) by using library functions such as OpenCV. Be sure to select enough corners in different locations and record their coordinates in the image.

3.Generate 3D points in object space: according to the selected corner coordinates, create a set of 3D points in the corresponding world coordinates, that is, the real location on the plate.

4.Generate two-dimensional points of the image plane: using the internal and external parameters of the camera, the world coordinates are converted to the image plane to get two-dimensional points. These points represent the position of the calibration plate in the image.

5.Solving camera parameters: using the method of minimizing reprojection error to estimate the internal and external parameters of the camera.

6.Test results: according to the experimental

results, the data are analyzed to verify the effect and accuracy of camera calibration.

The camera calibration method in this paper adopts the single-sided checkerboard method proposed by Zhang Zhengyou. First of all, make a piece of calibration checkered paper. As shown in figure 9, the grid number of the calibration grid paper is set to 7 × 9, and the size of each small grid is 50mm × 50mm. Huawei camera was used to take pictures of the calibrated grid paper from different angles, and a total of 16 photos were taken, as shown in figure 10.

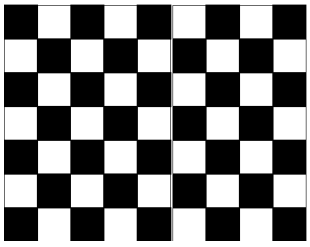

[Fig. 9] Calibration checkered paper

[Fig. 10] Total shot image

Matlab has a Camera Calibrator toolbox, which can check the pictures and get the main distance, main points and parameters of the camera. When all the images are read successfully, the corner extraction command can be executed to extract the corners of the black and white lattice of the image. This process requires manually clicking on the exact positions of the four edges and corners in each image, and then entering the dimensions dx and dy of each square in the grid in the X and Y directions for corner extraction, as shown in figure 11.

If the estimated corner is close to the corner position in the actual image, the corner extraction of the next image will be carried out. If there is a large deviation between the estimated corner position and the actual position, it will lead to wrong corner extraction.

If the photo angle problem is prompted, the corner position should be adjusted manually to avoid serious deviation in the experimental results.

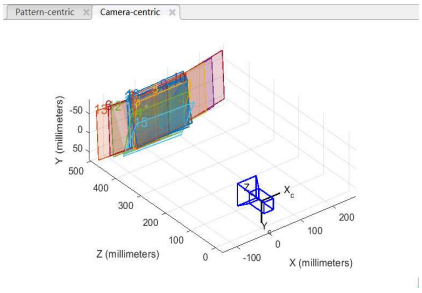

[Fig. 11] Corner extraction

After the corner extraction is completed, you can run "Calibration" for camera calibration. This calibration process is mainly completed by two steps: initial initialization and nonlinear optimization. In the initialization step, the calibration parameters are calculated in a closed loop, and this process does not include lens distortion. The nonlinear optimization process minimizes the overall mapping error for all calibration parameters. Optimization is to calculate the specific Jacobian matrix, then to the direction of gradient decline, and finally get the camera calibration result, as shown in figure 12.

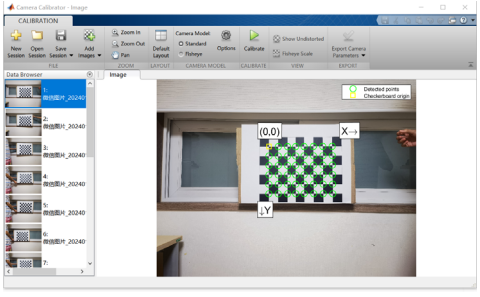

[Fig. 12] Calibrating experimental results

Click the "Show Extrinsic" command to see the 3D relationship between the camera and the calibration checkered paper, as shown in figure 13, which is exactly consistent with the actual spatial position of the photo.

The average reprojection error in this experiment is 5.22pixels , compared with the designed calibration paper, the size of each square is 50mm × 50mm, and the difference is 0.22pixels , the error is very small, as shown in figure 14.The reprojection error here refers to the difference between the projection of the real 3D space points on the image plane (that is, the pixels of the image) and the reprojection (the virtual pixels calculated in this experiment).

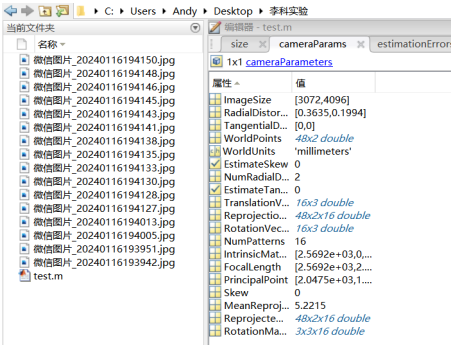

[Fig. 13] 3D relationship between camera and Calibration Checker Paper

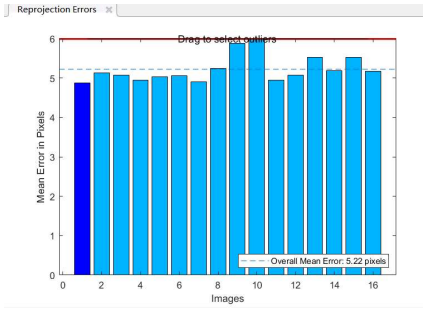

[Fig. 14] Error analysis

After we save the experimental results in the file "Calib_Result.mat" through "Save", we can get the camera's world coordinates, camera internal parameters, translation vectors and rotation matrices, as shown in figs. 15,16,17,18.

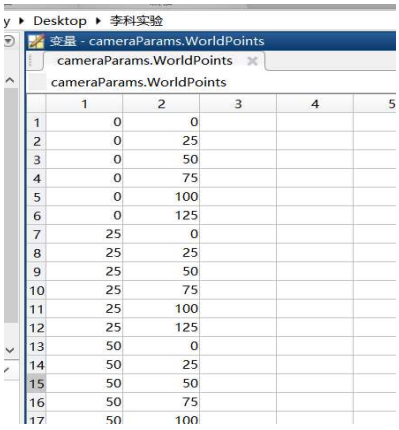

[Fig. 15] World coordinates of the camera

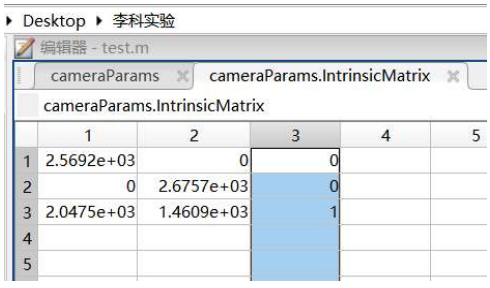

[Fig. 16] The internal parameters of the camera

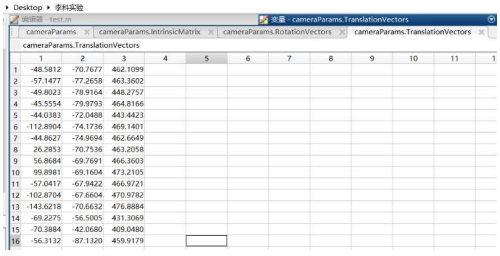

[Fig. 17] Translation vectors of photos

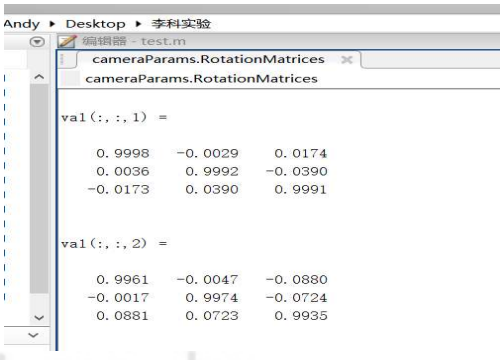

[Fig. 18] Rotation matrices of the photo

We select the two world coordinates of the origin (0,0) and the first photo (0,0.25), validate the algorithm formula in the third section as follows, and calculate the pixel coordinate system of the image. Let's first calculate the pixel coordinates of the origin (0,0) :

$$z_c\begin{bmatrix}u_1\\v_1\\1\end{bmatrix}=\begin{bmatrix}2569&0&2047&0\\0&2675&1461&0\\0&0&1&0\end{bmatrix}\begin{bmatrix}0.998&-0.0029&0.0174&-48.5812\\0&1&-0.0390&-70.7677\\-0.0173&0.0390&0.9991&462.1099\\0&0&0&1\end{bmatrix}\begin{bmatrix}0\\0\\0\\1\end{bmatrix}=\begin{bmatrix}821133.8625\\485838.9664\\462.1099\end{bmatrix} \tag{2.2}$$

Through the calculation by(2.2), it is known that the scale factor of the image coordinate origin is 462.1099. In order to make the third element 1, the results are all divided by the scale factor 462.1099 at the same time. Finally, the image coordinates of the origin(0,0) is as follows(2.3) :

$$\begin{cases}u_1\\v_1\end{cases}=\begin{bmatrix}1776.92\\1051.35\end{bmatrix} \tag{2.3}$$

Using scientific counting method to convert u1 and v1, the following formula (2.4) is obtained :

$$\begin{cases}u_1\\v_1\end{cases}=\begin{cases}1.77692e+03\\1.05135e+03\end{cases} \tag{2.4}$$

Then we calculate the pixel coordinates of the first photo (0,0.25) :

$$Zc\begin{bmatrix}u2\\v2\\1\end{bmatrix}=\begin{bmatrix}2569&0&2047&0\\0&2675&1461&0\\0&0&1&0\end{bmatrix}\begin{bmatrix}0.998&-0.0029&0.0174&-48.5812\\0&1&-0.0390&-70.7677\\-0.0173&0.0390&0.9991&462.1099\\0&0&0&1\end{bmatrix}\begin{bmatrix}0\\0\\0.25\\1\end{bmatrix}=\begin{bmatrix}821656.327075\\486177.806425\\462.359675\end{bmatrix} \tag{2.5}$$

Through the calculation by(2.5), it is found that the scale factor of the first photo is 462.359675. In order to make the third element 1, the results are all divided by the scale factor 462.359675. Finally, the image coordinates (0,0.25) of the first photo are as follows (2.6) :

$$\begin{cases}u_2\\v_2\end{cases}=\begin{bmatrix}1777.09\\1051.51\end{bmatrix} \tag{2.6}$$

Using scientific counting method to convert u2 and v2, the following formula is obtained (2.7) :

$$\begin{cases}u_2\\v_2\end{cases}=\begin{cases}1.7709e+03\\1.05151e+03\end{cases} \tag{2.7}$$

Finally, the coordinate values of formulas (2.4) and (2.7) are compared with the corresponding coordinates obtained by corner detection in the experiment (as shown in figure 19). The x-axis standard accuracy of u1 and u2 is respectively (1.77692-1.7740) /1.7740=99.84%、(1.7709-1.7740) /1.7740=99.83% , The standard accuracy of y-axis of u1 and u2 is respectively (1.05135-1.0459) /1.0459=99.48%、(1.05151-1.0459) /1.0459=99.46% , The error is very low.

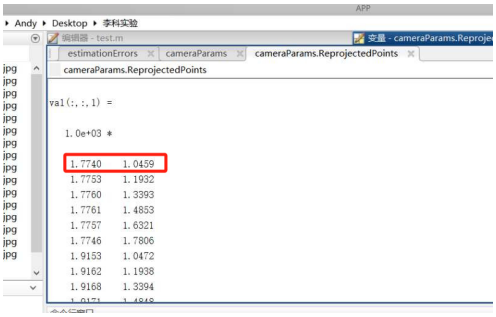

[Fig. 19] Obtaining coordinates of Corner Detection in experiment

According to the conversion relationship between image coordinates and pixel coordinates in figure 6, the pixel coordinates combined with the origin (0,0) are (1776.92, 1051.35),the pixel coordinates of the first photo (0,0.25) are (1777.09,1051.51),it can be concluded that the pixel coordinates of projection point $o(u_0, v_0)$ is u0=1051.51-1051.35=0.16mm , That is, the point changes from the 0.5mm size of the world coordinate system to the 0.16mm in the pixel coordinate system.

It can be calculated from the above that the actual size represented by a pixel is 0.5/0.16=3.12mm, indicating that the ratio of the world coordinate system to the pixel coordinate system is 0.5:0.16=0.16:1.

At the same time, the pixel coordinate of the origin (0,0) is (1.77692,1.05135),the pixel coordinates of the first photo (0,0.25) are (1.77709, 1.05151),the pixel coordinates of the projection point of the first photo (0,0.25) are (1.7740, 1.0459),the scale factor S of the actual measurement area and aerial view calculated by the substitution formula (1.8) is as follows :

$$S = \frac{\sqrt{(1.77692-1.77709)^2+(1.05135-1.05151)^2}}{1.774}$$
$$= \frac{\sqrt{(-0.00017)^2+(-0.00016)^2}}{1.774}$$
$$\equiv \frac{0.00023}{1.774} = 0.14$$

In this way, the calculated scale coefficient S=0.14 of the actual measurement area and the aerial view is in good agreement with the ratio of the world coordinates to the pixel coordinates.

Through the verification and data analysis of this experiment, we verify the conversion formula of each coordinate system in section 3, which fully illustrates the accuracy and practical operation of each formula.

5. Video spatialization algorithm and its application

Video spatialization means that the pixel coordinates of the video image are converted into geo-spatial coordinates, which is convenient for the superimposed display of video and GIS data, and the corresponding position of the object in the video is obtained [20]. That is, using the principle of keyhole imaging and coordinate system transformation, the conversion model between video image pixels and geo-spatial coordinates is established by calibration, so that any point on the video image has spatial coordinate information, and the video spatial position intelligence is constructed. to achieve alarm location.

5.1 Transformation of image pixel coordinates to longitude and latitude coordinates

In the real application scenario, after we calibrate the head and calculate the parameters needed by the algorithm, we can carry out video spatialization related applications.

Click anywhere on the video screen to calculate the spatial geographical coordinates. The algorithm description process is shown in figure 20 :

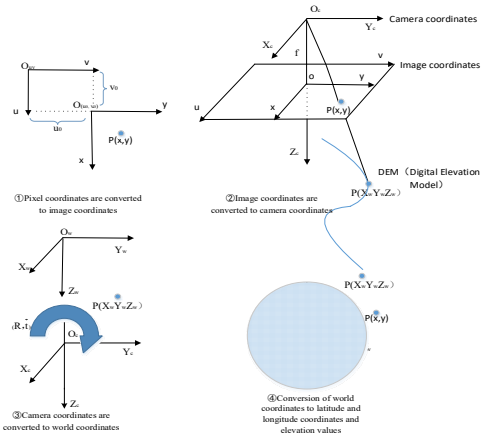

[Fig. 20] The conversion process of image pixel coordinates to longitude and latitude coordinates

①Click on the p point on the video screen to obtain the pixel coordinate p (u,v) of the p point. Through the pixel coordinates to image coordinates algorithm, the coordinate in pixels is converted into the image coordinate p (x,y) in physical size meters;

②In the camera coordinate system, the length of the origin O_c-o of the two coordinate systems is zf, so the coordinates of the p point in the camera coordinate system can be obtained directly (x,y,zf) ,through the O_{cp}, the coordinates of the point can be calculated by increasing the unit distance outward, and then the coordinate y value of the point is compared with the DEM elevation value of the terrain.If it is less than the elevation value, it is considered to intersect, that is, point $P(X_wP, Y_wP, Z_wP)$. Otherwise, continue to increase the unit distance calculation until the total distance exceeds the camera visual distance ;

③By rotating the horizontal angle, pitch angle and roll angle of the camera, then rotating the longitude and latitude of the camera, and finally translating to the position of the spherical center, the calculated P-point coordinates are transformed into the world coordinates with the spherical center as the origin ;

④Through the algorithm of turning longitude and latitude coordinates in the world coordinates, the P point coordinates are transformed into longitude and latitude coordinates and elevation values.

5.2 Fusion of geospatial vector data and video scene

The vector data in the geographical space, such as the layer of the mine distribution area in Pingxiang City, is dynamically drawn to the video picture in real time and fused with the video scene. The algorithm description process is shown in figure 21 :

①The longitude and latitude of the four corners of the current picture are calculated by changing the image pixel coordinates to latitude and longitude coordinates, and then the four corners are merged into a polygon and the mine layer for spatial calculation, the intersecting parcels are calculated, and then the longitude and latitude coordinate sets of the parcels are obtained ;

②Convert the parcel coordinate set and camera position into world coordinates, taking the point P in the parcel coordinate set as an example ;

③Translate and rotate the P-point world coordinates relative to the camera world coordinates to the camera coordinates ;

④Convert P-point camera coordinates to image coordinates p-point ;

⑤Convert image coordinates p points to pixel coordinates ;

⑥Draw points and connect lines on the video screen based on pixel coordinates, and finally realize the fusion of geospatial vector data and video scene.

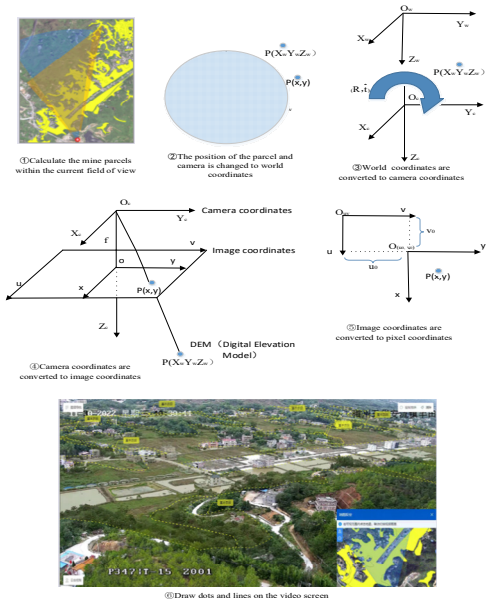

[Fig. 21] The Fusion process of Geospatial Vector data and Video reality

5.3 Application and verification of practical cases

Taking Pingxiang area of Jiangxi Province as the research object, "Dingrun Mining", one of the 41 open-pit mines under supervision, is selected as the monitoring point under the actual scene, and the construction machinery is selected to identify and track the excavator. Select the nearby high point monitoring of the communication operator's base station, as shown in figure 22.

[Fig. 22] The high point monitoring of the communication operator's base station

Generate the head calibration interface of "Dingrun Mining" according to sections 5.1 and 5.2, as shown in figure 23.

It should be noted that the horizontal angle and pitch angle reported after the installation of the equipment is a relative value without direction, that is, the equipment needs to be adjusted to zero degrees in the direction of due north and east, so as to ensure the angle of the direction of due north and east, keep parallel with X_w, Y_w.

In addition, we select 9 groups of reference points, each of which includes horizontal angle, pitch angle, multiple distance, picture capture, position of reference point in the picture, longitude and latitude coordinates of reference point, etc., to provide a fixed reference boundary for drawing the actual measurement area, and then draw the final boundary of the legal mining area of "Dingrun Mining", as shown in figure 24.

[Fig. 23] The cloud platform calibration interface of "Dingrun Mining"

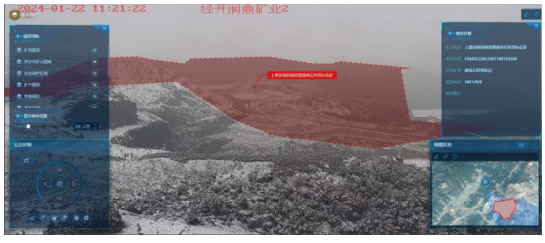

[Fig. 24] The boundary of the mining area legally mined by "Dingrun Mining“

During the period from 9:30 to 9:40 on January 18, 2024, Dingrun Mining was monitored in real time by high point video, and a total of 176 monitoring pictures were saved, as shown in figures 25,26.

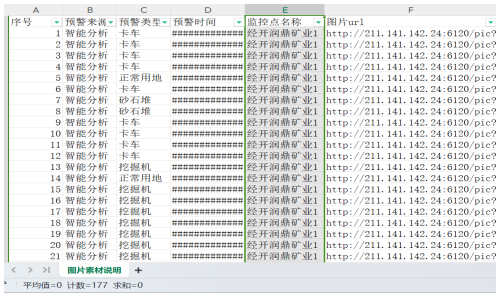

序号	预警来源	预警类型	预警时间	监控点名称	图片url
1	智能分析	卡车	##########	经开润鼎矿业1	http://211.141.142.24:6120/pic?
2	智能分析	卡车	##########	经开润鼎矿业1	http://211.141.142.24:6120/pic?
3	智能分析	卡车	##########	经开润鼎矿业1	http://211.141.142.24:6120/pic?
4	智能分析	卡车	##########	经开润鼎矿业1	http://211.141.142.24:6120/pic?
5	智能分析	正常用地	##########	经开润鼎矿业1	http://211.141.142.24:6120/pic?
6	智能分析	卡车	##########	经开润鼎矿业1	http://211.141.142.24:6120/pic?
7	智能分析	砂石堆	##########	经开润鼎矿业1	http://211.141.142.24:6120/pic?
8	智能分析	砂石堆	##########	经开润鼎矿业1	http://211.141.142.24:6120/pic?
9	智能分析	卡车	##########	经开润鼎矿业1	http://211.141.142.24:6120/pic?
10	智能分析	卡车	##########	经开润鼎矿业1	http://211.141.142.24:6120/pic?
11	智能分析	卡车	##########	经开润鼎矿业1	http://211.141.142.24:6120/pic?
12	智能分析	卡车	##########	经开润鼎矿业1	http://211.141.142.24:6120/pic?
13	智能分析	挖掘机	##########	经开润鼎矿业1	http://211.141.142.24:6120/pic?
14	智能分析	正常用地	##########	经开润鼎矿业1	http://211.141.142.24:6120/pic?
15	智能分析	挖掘机	##########	经开润鼎矿业1	http://211.141.142.24:6120/pic?
16	智能分析	挖掘机	##########	经开润鼎矿业1	http://211.141.142.24:6120/pic?
17	智能分析	挖掘机	##########	经开润鼎矿业1	http://211.141.142.24:6120/pic?
18	智能分析	挖掘机	##########	经开润鼎矿业1	http://211.141.142.24:6120/pic?
19	智能分析	挖掘机	##########	经开润鼎矿业1	http://211.141.142.24:6120/pic?
20	智能分析	挖掘机	##########	经开润鼎矿业1	http://211.141.142.24:6120/pic?
21	智能分析	挖掘机	##########	经开润鼎矿业1	http://211.141.142.24:6120/pic?

[Fig. 25] Picture list of "Dingrun Mining" during the monitoring period

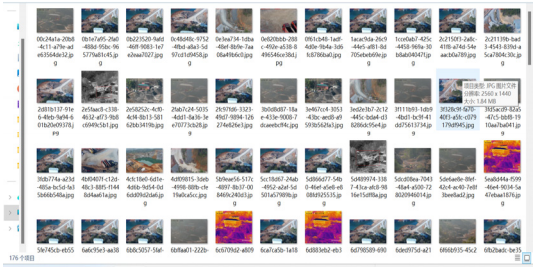

[Fig. 26] Real picture of "Dingrun Mining" during the monitoring period

In the early warning system, the legal mining area boundary and location of "Dingrun Mining" are shown in figure 27.

9:39:48 on January 18, 2024, excavator equipment was detected for cross-border mining. As shown in figure 28, according to the PNPoly algorithm design in section 3.6, it is calculated that there is an intersection between the coordinates of the monitoring point and the reference boundary of the actual measurement area, and the existence of cross-border mining behavior is determined, and an alarm is triggered and early warning information is sent to the site supervisor, as shown in figure 29, 30, 31.

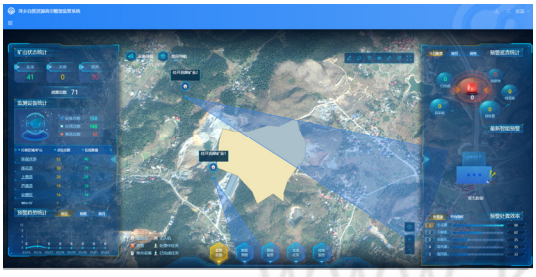

[Fig. 27] Mine early warning system

[Fig. 28] The target to be monitored intersects with the boundary of the mining area

[Fig. 29] Trigger an alarm after an out-of-line behavior occurs

[Fig. 30] The early warning information is sent to the on-site supervisors

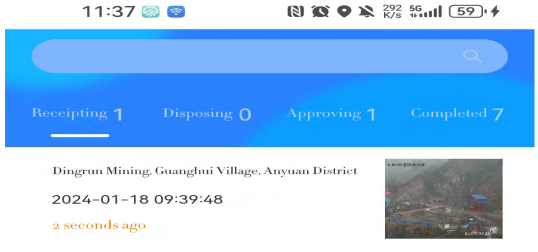

[Fig. 31] The early warning information has been sent to the on-site supervisors

To sum up, we can realize the closed-loop management of the whole process of cross-border mining early warning.

6. Conclusion

Through the research and realization of photogrammetry technology and Zhang Zhengyou calibration method, this paper creatively deduces the coordinate transformation relationship between the aerial view coordinates of the video angle and the actual measurement area. on the basis of verifying the camera calibration experiment, a video spatialization algorithm is constructed to identify and track mining construction machinery, and an intelligent early warning system for cross-border mining in open-pit mines is studied and designed. It is of great practical significance for the monitoring and early warning of open-pit mines to realize the monitoring and early warning of open-pit mines under the background of regular manual verification of illegal mining and illegal mining in open-pit mines.

The field experiments show that the operation of the system is stable and reliable, and the target tracking accuracy of the verification system is high, which can effectively improve the early warning ability of cross-border mining in open-pit mines, and greatly reduce the labor cost of cross-border mining supervision in open-pit mines. improve the timeliness and accuracy of mining supervision.

References

[1] W.J.Song, Sh.Zh.Li and T.Min, "Research and implementation of remote Monitoring system for Mineral Resources Mining," Scientific and technological management of land and resources, Vol.30, No.3, pp.93-97, 2013.

[2] J.K. Liu, "Remote sensing monitoring and analysis of mine geological mining based on geophysical technology," World non-ferrous metals, Vol.18, No.22, pp.27-29, 2018.

[3] Pingxiang Local Chronicles compilation Committee, "Pingxiang City Chronicles," China: local Records Publishing House, pp.12-45, 2007.

[4] H.K.Lin, "Motion state analysis and recognition of excavator in complex scene," Guangzhou: South China Agricultural University, 2016 .

[5] Zh.Y.Zhang, "A Flexible New Technique for Camera Calibration," IEEE Tran sactions on Pattern Analysis & Machine Intelligence, Vol.22, No.11, pp.1330-1334, 2000.

[6] L.X.Wu, "Progress of digital mines in China," Geographic information world, Vol.6, No.5, pp.6-13, 2008.

[7] J.Y.Gong, "Development opportunities and challenges of surveying and Mapping remote Sensing Technology in the era of artificial Intelligence," Journal of Wuhan University Information Science Edition, Vol.43, No.12, pp. 1788-1796, 2018.

[8] C.B.Choy, D.F.Xu, Gwak J., K.Chen and Savarese S, "A unified approach for single and multi-view 3D object reconstruction," in Proceedings of 2016 European Conference on Computer Vision, Amsterdam, 2016, pp.628-644. Dissertations.

[9] B.Yang, Stefano R and Andrew M, "Dense 3D Object Reconstruction from a Single Depth View," IEEE transactions on pattern analysis and machine intelligence,Vol.41, No.12, pp.2820-2834.

[10] S.K.Liu, Giles L and Ororbia A, "Learning a hierarchical latent variable model of 3D shapes," in Proceedings of 2018 International Conference on 3D Vision, Italy, 2018, pp.542-551. Dissertations.

[11] Tulsiani S, Efros A.A and Malik J, "Multi-view consistency as supervisory signal for learning shape and pose prediction," in Proceedings of 2018 IEEE/CVF Conference on Computer Vision and Pattern Recognition, USA, 2018, pp.2897-2905. Dissertations.

[12] H.Yu and J.Oh, "Anytime 3D object reconstruction using multi modal variational autoencoder," IEEE Robotics and Automation Leters, Vol.7, No.02, pp.2162-2169, 2022.

[13] L.Feng, J.S.Xie and G.Li, "Summary of the principles and methods of camera calibration," Mechanical Engineer, Vol.16, No.01, pp.18-20, 2016.

[14] Y.Chai and J.K.Xu, "Target recognition and location system based on machine vision," Computer engineering and design, Vol.40, No.12, pp.3557-3562, 2019.

[15] Z.M.Pan, K.W.Jin and K.X.Pan, "Research on keyhole imaging," Physics and engineering, Vol.28,No.4, pp.102-108, 2018.

[16] M.W.Zhang, W.T.Leng and H.Shen, "Determination of the position relationship between privacy-protected points and arbitrary polygons," Journal of cryptography, Vol.6, No.04, pp.443-454, 2019 .

[17] L.Lv, T.Z,Yao and J.T.Song, "Design and implementation of 3D reconstruction system based on monocular vision," Computer engineering, Vol.44, No.12, pp.233-239, 2018.

[18] F.Yang, "Research on large-field-of-view camera calibration technology for large aeronautical component measurement," Dalian University of Technology, 2017.

[19] Y.L Ji, H.T Duan. "Research on key Technologies of Video Image Analysis in Intelligent Video Surveillance system," China's informationization, Vol.19, No.02, pp.46-49, 2019.

[20] R.Zh.Guo, H.T.Lin and B.He, "GIS framework for smart city," Journal of Wuhan University, Vol.45, No.12, pp.1829-1835, 2020.

이 크(Li Ke) [정회원]

- June 2013, East China Jiaotong University School of Software (Bachelor of Engineering)
- June 2016, East China Jiaotong University School of Software (Master of Engineering)
- January 2022 - Present, has been pursuing Ph.D. in Intelligent Fusion in IT at Mokwon Universit(Student)

〈관심분야〉

Information theory and their applications,Image recognition and analysis

민 병 원(Byung-Won Min) [정회원]

- He received M.S. degree in computer software from Chungang University, Seoul, Korea in 2005.
- He received Ph.D. degree in the dept. of Information and Communication Engineering, Mokwon University, Daejeon, Korea, in 2010.
- He is currently a professor of Mokwon University since 2010.

〈관심분야〉

digital communication systems, Big Data